Confirmation for and Predictability of Distinct U.S. Impacts of El Niño Flavors

TAO ZHANG

Cooperative Institute for Research in Environmental Sciences, University of Colorado Boulder, and NOAA/Physical Sciences Laboratory, Boulder, Colorado

MARTIN P. HOERLING, ANDREW HOELL, AND JUDITH PERLWITZ

NOAA/Physical Sciences Laboratory, Boulder, Colorado

JON EISCHEID

Cooperative Institute for Research in Environmental Sciences, University of Colorado Boulder, and NOAA/Physical Sciences Laboratory, Boulder, Colorado

(Manuscript received 23 October 2019, in final form 14 April 2020)

ABSTRACT

Whether distinct wintertime U.S. climate conditions exist for central-Pacific (CP) versus eastern-Pacific (EP) El Niño events is explored using atmospheric and coupled ocean–atmospheric models. Results using the former agree with most prior studies indicating different U.S. temperature and precipitation patterns associated with El Niño flavors. Causes are traced to equatorial rainfall sensitivity to both magnitudes and spatial patterns of sea surface temperatures (SSTs) distinguishing CP and EP cases. Warmer east equatorial Pacific Ocean SSTs during EP than CP events, specifically for strong EP cases, are responsible for greater east equatorial Pacific rainfall, which displaces tropospheric circulation anomalies eastward over the Pacific–North American region. Weak-amplitude EP cases and all CP events since 1980 fail to excite east equatorial Pacific rainfall, thus not initiating the dynamical chain of effects characterizing strong EP cases. Over the contiguous United States, the difference in tropospheric circulations between strong EP and CP events describes a cyclonic pattern that renders the former colder and wetter. Regional signals include notably colder western and warmer eastern U.S. surface temperatures during EP versus CP events, and higher southwestern and southeastern U.S. precipitation during EP events. We demonstrate the important result—new to studies of observed El Niño flavor impacts—that coupled models largely reproduce the sensitivities of atmospheric models. Confirmed hereby is the realism of prior estimates of El Niño flavor impacts that relied on atmospheric models alone. We further examine predictability of El Niño flavors using coupled forecasts, demonstrating that SST distinctions between CP and EP events and their diverse U.S. wintertime impacts are predictable at least a season in advance.

1. Introduction

The coupled atmosphere–ocean variability associated with El Niño–Southern Oscillation (ENSO) has widespread effects on surface climate across the globe (e.g., Ropelewski and Halpert 1986; Kiladis and Diaz 1989). Indeed, the sea surface temperature (SST) variability related to El Niño constitutes the principal source of seasonal forecast skill for surface temperature and precipitation for the contiguous United States (e.g., Hoerling et al. 1997; Quan et al. 2006; Zhang et al. 2016, 2018; Huang et al. 2019). The historical composite of positive phase ENSO-related climate anomalies is characterized by warm and dry conditions over the northern United States and cold and wet conditions over the southern United States, a pattern often observed during the winter season. While Quan et al. (2006) suggest that a single pattern of the ENSO climate signal explains the source for U.S. temperature and precipitation skill, on average, subsequent studies have identified different climate signals associated with so-called

Supplemental information related to this paper is available at the Journals Online website: https://doi.org/10.1175/JCLI-D-19-0802.s1.

Corresponding author: Dr. Tao Zhang, tao.zhang@noaa.gov

DOI: 10.1175/JCLI-D-19-0802.1

flavors of El Niño (e.g., Mo 2010; Yu et al. 2012; Guo et al. 2017; Zhang et al. 2016, 2018), raising the question of whether additional skill sources beyond that derived from a sole composite pattern exist.

The canonical view of mature El Niño events is of tropical Pacific Ocean SSTs having maximum positive anomalies over the eastern equatorial Pacific Ocean (Rasmusson and Carpenter 1982), warm events that have subsequently been referred to as eastern-Pacific (EP) El Niño events. More recent studies have shown a different type of SST warming pattern, one in which tropical Pacific SSTs have their maximum positive anomalies confined to the central equatorial Pacific. This latter structure has been variously termed the central-Pacific (CP) El Niño (Kao and Yu 2009), Date Line El Niño (Larkin and Harrison 2005), El Niño Modoki (Ashok et al. 2007), or warm pool El Niño (Kug et al. 2009). It has become well recognized, however, that ENSO exhibits a continuum of flavors, being neither solely CP- nor EP-type events but involving various combinations of CP and EP, an empirical result also confirmed by coupled atmosphere–ocean simulations (Capotondi et al. 2015). Nonetheless, both observations and models suggest a clustering of events having their maximum SST anomalies either in the eastern or the central equatorial Pacific, and in which the magnitude of SST warming increases as the longitude of peak SST anomalies shifts eastward (Capotondi et al. 2015).

A classic problem in climate dynamics concerns the sensitivity to such different patterns of tropical SST variability. First posed by Horel and Wallace (1981), who had identified a single composite of the planetary-scale atmospheric phenomena associated with ENSO, the authors made the following conjecture: ''[i]f these patterns [i.e. the linear correlation of upper air geopotential heights with indices of ENSO-related tropical forcing] constitute blurred images resulting from our inadvertent superposition of an ensemble of sharper patterns, corresponding to the various states of the equatorial atmosphere that have existed under the general category of 'warm episodes', then there is hope that given a more specific and detailed prediction of tropical sea surface temperatures and rainfall patterns, it might be possible to use simplified numerical models...to infer midlatitude climate anomalies with a higher degree of detail and accuracy than is now possible'' (p. 828). Subsequent studies using numerical models of varying complexity have revealed that the atmospheric circulation response to El Niño should vary from event to event depending on the position and magnitude of tropical Pacific SST anomalies (e.g., Barsugli and Sardeshmukh 2002; Hoerling and Kumar 2002), leaving open the prospect for improved seasonal predictions beyond the use of a single response pattern. It is with the hope for improving forecasts, articulated by Horel and Wallace, that we now proceed to re-examine the classic problem of ENSO-related climate variability using modern numerical models employed in climate research and prediction science.

What is new in the approach taken herein is that parallel sets of atmospheric and coupled ocean–atmospheric model experiments are used 1) to explore further whether there is a basis for the existence of distinct U.S. climate patterns related to the different expressions of El Niño SSTs and 2) to establish that El Niño flavor impacts that have extensively relied on atmospheric model experimentation are a faithful and accurate representation of the sensitivity occurring in the fully coupled system. The coupled model experiments are derived from an initialized seasonal forecast system, and the hindcasts of those for the historical period of 1980–2016 are used to both validate the sensitivity of our atmospheric model subjected to the observed sea surface temperatures [Atmospheric Model Intercomparison Project (AMIP)] and also to explore the lead time–dependent predictability of distinct U.S. impacts of El Niño diversity.

While observational composites for diverse El Niño warming patterns exhibit different U.S. climate anomalies (e.g., Mo 2010), these may arise more from internal atmospheric dynamics (i.e., sampling noise) than from sensitivities to forcing effects of coupled ocean–atmosphere variability (Deser et al. 2018). Here we employ multimodel large ensemble atmospheric simulations and build upon prior modeling studies that used appreciably smaller ensemble sizes, thereby minimizing a confounding of forced signal with sampling noise (Guo et al. 2017). Furthermore, the experiments examined herein use the actual observed historical SST variability, thereby going beyond prior model sensitivity studies that employed idealized SST patterns (e.g., Yu et al. 2012; Yu and Zou 2013; Garfinkel et al. 2013).

An overview of the various findings from previous studies will help to place into context our own results concerning the U.S. impacts of El Niño flavors. Based on atmospheric model experiments forced by idealized SST anomalies representative of CP and EP spatial structures, Yu et al. (2012) and Garfinkel et al. (2013) found EP events to be colder over the western United States overall, with Yu et al. further noting that the eastern United States was also warmer under the influence of EP forcing. Regarding precipitation, Yu and Zou (2013) and Garfinkel et al. (2013) both found the Pacific Northwest to be wetter but the Southwest to be drier in EP versus CP forcing scenarios. Based on atmospheric model experiments forced by realistic observed SST

variability, Hu et al. (2012) and Garfinkel et al. (2019) produced broadly similar temperature signals over the United States to the experiments using idealized forcing. Regarding precipitation, the results from realistic SST experiments compare less favorably with the results from experiments using idealized SST forcing. In particular, the U.S. Southwest was found to be wetter under EP forcing.

In synthesis, the U.S. precipitation patterns, and the distinction of EP versus CP U.S. signals in particular, appear to be more sensitive to details in the treatment of the SST forcing than the U.S. temperature patterns are. But it is important to note that these various signals have all been identified by stand-alone atmospheric models and have not been confirmed by parallel coupled ocean–atmosphere model systems. Recognizing that it has been unclear whether results from such uncoupled experiments are indicative of the physics of coupled air–sea interaction, we undertook for the first time an approach of examining parallel uncoupled and coupled experiments involving virtually identical El Niño SST conditions. Also key in this new approach is that the coupled forecast system utilizes a nearly identical atmospheric dynamical component to the uncoupled atmospheric model.

Our paper is organized as follows. Section 2 describes the observational and model datasets as well as the methodology of our analysis. Section 3 first presents the observed climate anomalies linked to two types of El Niño and then the corresponding response to the SST forcing associated with each type based on AMIP simulations. Last, the predictability of El Niño flavors and their U.S. impacts are investigated in seasonal forecasts. A summary of principal findings and a discussion of broader implications are given in section 4.

2. Datasets and methods

Observed estimates for U.S. climate conditions associated with El Niño variability during the Northern Hemisphere (NH) December–February (DJF) winter season are based on the Global Historical Climatology Network/Climate Anomaly Monitoring System (GHCN/CAMS) 2-m temperature (Fan and van den Dool 2008) and gauge-based gridded monthly Global Precipitation Climatology Centre (GPCC) datasets (Schneider et al. 2014), available at 1° by 1° resolution. To provide an understanding of the possible tropical driver for the U.S. conditions, we also present a global view of SST and precipitation fields. Estimates of observed SST variability are from the Hurrell dataset (Hurrell et al. 2008), which is a combined version of the Hadley Centre's SST, version 1.1 (HadISST1), and the NOAA Optimal Interpolation (OI) SST version 2 (OIv2) from November 1981 onward. Global precipitation fields are from the Climate Prediction Center (CPC) Merged Analysis of Precipitation (CMAP; Xie and Arkin 1997) and are available at 2.5° by 2.5° resolution. Estimates of the observed upper-level circulation pattern are derived from analysis of 200-hPa geopotential height fields using the National Centers for Environmental Prediction (NCEP)–National Center for Atmospheric Research (NCAR) reanalysis product (Kalnay et al. 1996).

For this study, the focus is on the U.S. impacts of the EP and CP El Niño types during the winter season for 1979–2016. EP and CP El Niño types are identified using a two-step approach. First, El Niño winters are defined to occur when the SST anomaly of the Niño-3.4 index exceeds 0.5°C during DJF relative to a 1981–2010 climatology. Second, El Niño winters are defined as EP or CP based on the majority approach introduced by Yu et al. (2012). A winter is determined to be EP or CP if at least two of three of the following metrics determine as such: the El Niño Modoki index (EMI) method[1] of Ashok et al. (2007), the Niño method[2] of Yeh et al. (2009), and the EP/CP index method[3] of Kao and Yu (2009). As shown in Table 1, three of the 11 El Niño events since 1979 are of the EP type (1982/83, 1997/98, 2006/07), and eight of them are of the CP type (1986/87, 1987/88, 1991/92, 1994/95, 2002/03, 2009/10, 2014/15, 2015/16). The classification of these EP and CP El Niño events is generally consistent with the findings of Yu et al. (2012) from 1979 to 2012, although different SST data are used and a different analysis period is discussed. To provide a visual indication of how these 11

[1] For the EMI method, EMI is represented by the second mode of empirical orthogonal function (EOF) analysis of the tropical Pacific SST anomaly (SSTA) and is defined as SSTc − 0.5(SSTe + SSTw), where SSTc, SSTe, and SSTw are the average SSTA over the central equatorial Pacific and eastern and western regions of the tropical Pacific, respectively. El Niño events are identified as CP type when the DJF EMI values are equal to or greater than 0.7 STD, where STD is the DJF standard deviation of the EMI. Otherwise, El Niño events are identified as EP type.

[2] For the Niño method, El Niño events are classified as CP or EP types when the values of the DJF Niño-4 index are respectively greater than or less than the values of the DJF Niño-3 index.

[3] For the EP/CP-index method, a regression–EOF analysis is used to identify the CP and EP types of El Niño. The CP El Niño index is represented by the leading principal component of the EOF analysis of the SSTA after the regression of the SSTA onto the Niño-1+2 index, which is associated with eastern Pacific warming, is removed from the total SSTA field. The EP El Niño index is represented by the leading principal component of the EOF analysis of the SSTA after the regression of the SSTA onto the Niño-4 index, which is associated with central Pacific warming, is removed from the total SSTA field. El Niño events are considered to be CP or EP types when the values of the DJF CP index are respectively greater than or less than those of the DJF EP index.

TABLE 1. El Niño events since 1979 and their classification as based on the majority consensus from three different identification methods including the Niño method (Yeh et al. 2009), EMI method (Ashok et al. 2007), and EP/CP-index method (Kao and Yu 2009).

El Niño events	Classification method			
	Niño-3/4 method	EMI method	EP/CP method	Consensus
1982/83	EP	EP	EP	EP
1986/87	EP	CP	CP	CP
1987/88	CP	EP	CP	CP
1991/92	EP	CP	CP	CP
1994/95	CP	CP	CP	CP
1997/98	EP	EP	EP	EP
2002/03	CP	CP	CP	CP
2006/07	EP	EP	CP	EP
2009/10	CP	CP	CP	CP
2014/15	CP	CP	CP	CP
2015/16	EP	CP	CP	CP

El Niño events compare in their patterns—magnitudes and spatial structures—the left panel of Fig. 1 shows the zonal profile of their respective SST anomalies along the equatorial Pacific, ranking their strengths in the order of the Niño-3.4 index. Clearly, the longitude of maximum SST warming during EP events is shifted eastward compared to CP events. Except for 2006/07 and 2015/16 events, weak El Niño events as estimated from Niño-3.4 conditions alone tend to be CP type, whereas strong El Niño events tend to be EP type.

We examine the response to El Niño flavors using large ensembles of atmospheric model simulations, integrated under an AMIP protocol, to effectively separate atmospheric signals from internal atmospheric variability. One 50-member ensemble is based on the NCEP GFSv2, which has been extensively used in prior studies (e.g., Hoerling et al. 2013; Hartmann 2015; Hoell et al. 2016, 2017, 2018; Zhang et al. 2016, 2018). As the atmospheric component of the NCEP CFSv2 (Saha et al. 2014), the GFSv2 model is run at spectral T126 horizontal resolution with 64 vertical levels and forced with specified observed monthly varying SSTs and sea ice (Hurrell et al. 2008) and carbon dioxide concentrations for 1979–2018. Another 40-member ensemble is based on the NCAR Community Atmosphere Model, version 5 (CAM5; Neale et al. 2012). The CAM5 model was run at ~1° horizontal resolution with 30 vertical levels. The CAM5 AMIP ensemble was produced for the period 1901–2018 using the same observed SST and sea ice dataset as GFSv2 (Hurrell et al. 2008), historical atmospheric forcing for 1901–2005, and the representative concentration pathway 6.0 thereafter. Both AMIP ensembles are available online at the Facility for Climate Assessments (FACTS) (see https://www.esrl.noaa.gov/psd/repository/alias/facts). Anomalies are calculated relative to a 1981–2010 reference period for AMIP simulations and observations.

To test the robustness of the AMIP simulated sensitivities and to examine the predictability of El Niño diversity, ensembles from a coupled ocean–atmosphere model are also examined. The data are from the NOAA Climate Forecast System version 2 (CFSv2) hindcasts (Saha et al. 2014), the atmospheric component of which (GFSv2) is that used in the aforementioned AMIP experiments. The hindcasts are initialized every fifth day of a calendar month and comprise a 24-member ensemble for 1982–2018. We consider all DJF forecasts at 0-month lead (November start days) to 6-month lead (May start days). The anomalies of the CFSv2 reforecasts are calculated based on a lead-time-dependent model climatology (1982–2011). Biases in the SST climatology evolve quickly in the forecast cycle, the Pacific basin pattern of which consists of excessively cold conditions in the Niño-3 region, and excessive warmth in Niño-1+2 and Niño-4 regions (see Fig. S1 in the online supplemental material).

3. Results

a. *Observed composite anomalies for CP and EP El Niño events*

Figure 2 displays the wintertime observed anomalies related to EP (top) and CP (middle) El Niño events. As was already apparent from the zonal SST profiles in Fig. 1, the EP El Niño composite shows larger magnitude warm SST anomalies over the eastern equatorial Pacific compared to the CP composite (bottom left column). The SST difference between EP and CP composites is characterized by a zonal dipole pattern with large positive anomalies in the far eastern Pacific and slight negative anomalies in the central Pacific, consistent with the different centers of action of these two event types.

The EP versus CP composite differences in tropical Pacific rainfall (Fig. 2, bottom middle column) largely follow the differences in their SSTs—the maximum positive precipitation anomaly is shifted farther eastward in the EP compared to the CP composite. We note that the differences in tropical precipitation between these two types of El Niño are comparable to the magnitude of anomalies for the CP El Niño composite itself. These principal structural differences are found to be statistically significant, consistent with a known strong constraint that seasonal SST anomalies exert on rainfall over much of the tropical Pacific (Stern and Miyakoda 1995; Hoerling and Kumar 2002).

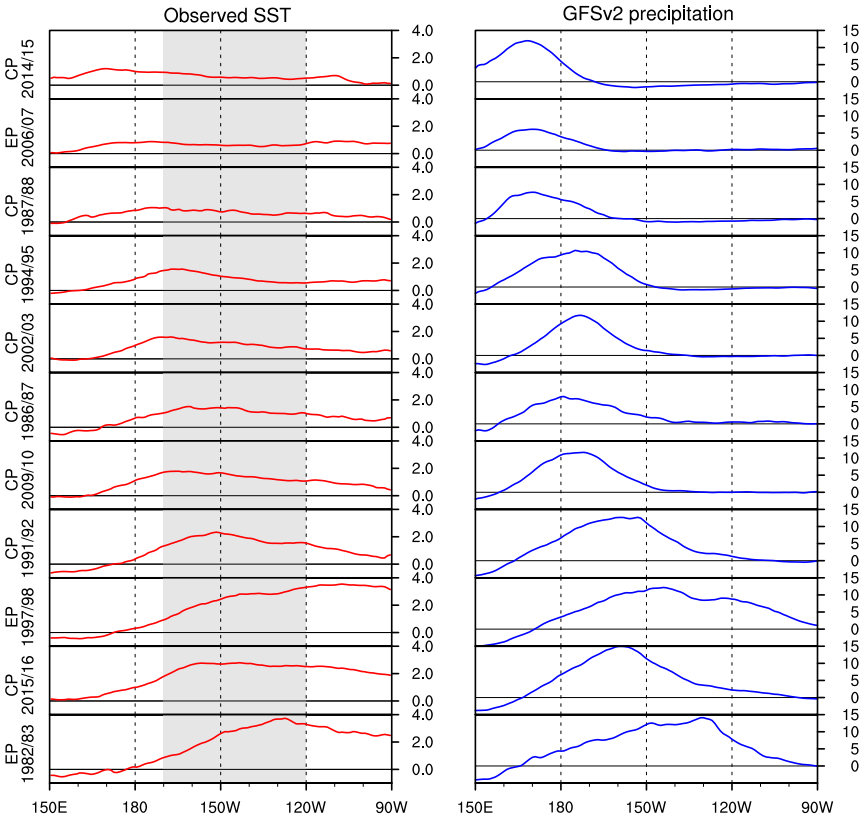

FIG. 1. (left) Zonal profiles of observed DJF SST anomalies (°C) averaged over the equator (5°N–5°S) for 11 El Niño events shown in Table 1. We use Niño-3.4 SST index to sort events from top to bottom and the consensus method to determine the El Niño type. The gray band shows the zonal range (170°–120°W) of the Niño-3.4 region. (right) Corresponding zonal profiles of GFSv2 simulated 50-member ensemble mean DJF precipitation anomalies (mm day^{-1}).

The upper-tropospheric circulation anomaly composites (Fig. 2, right column) for both EP and CP events bear the signature of the classic El Niño–related teleconnection pattern (e.g., Horel and Wallace 1981). This consists of anomalous subtropical anticyclones, cyclonic anomalies over the North Pacific and anticyclonic anomalies over the North American continent. The two wave trains are phase shifted, with their difference being characterized by an eastward displacement of the EP teleconnection relative to its CP counterpart (bottom right column). Such a displacement is consistent with dynamical understanding of the sensitivity of extratropical circulation responses to the location of tropical Pacific diabatic heating anomalies (e.g., Ting and Sardeshmukh 1993).

Given these differences in composite circulation anomalies, it is not surprising to find contrasting patterns of CP versus EP observed composite U.S. temperature (Fig. 3, left) and precipitation anomalies (Fig. 3, right). Both composites reveal greater warmth over the northern compared to the southern United States. Differences in their temperatures (bottom left) highlight the contrast in their west–east patterns with EP colder in the west and warmer in the east, a similar feature to those noted in the previous observational estimates using the analysis of a longer record (e.g., Yu et al. 2012; Deser et al. 2018). The precipitation patterns for both composites are wet in the southern United States. Their difference highlights the larger magnitude of wet anomalies spanning most of the contiguous United States in the EP composite (bottom right). This increased wetness of EP events is statistically significant over the Great Plains region, but differences are otherwise statistically insignificant over most of the contiguous United States. We also note that despite a broad similarity over the south central and southeastern United States, the precipitation difference over the southwestern United States is found to have a sign opposite to the prior observations based on a longer record (e.g., Yu and Zou 2013; Deser et al. 2018). The composite differences for surface temperature are not

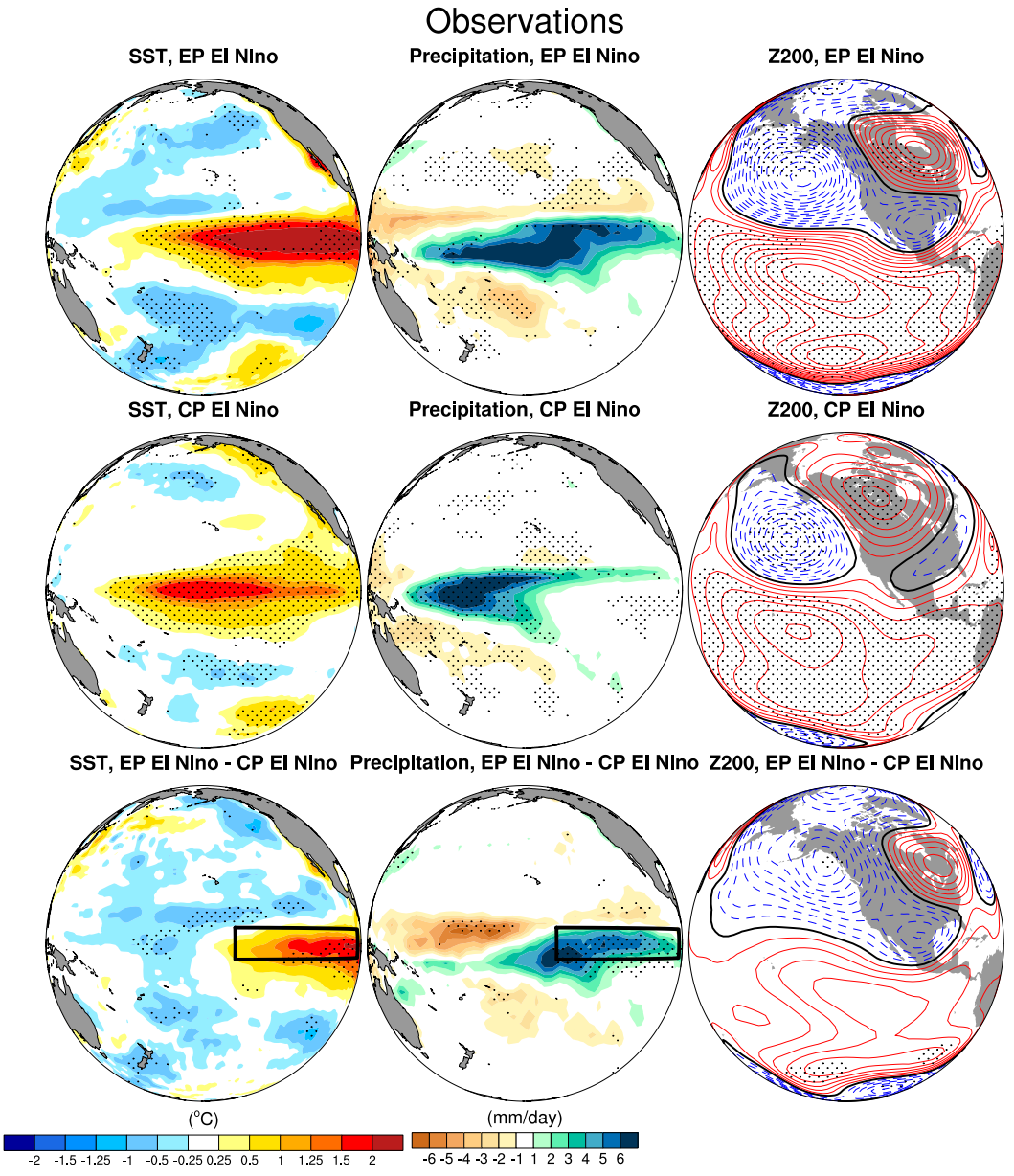

FIG. 2. Composite of observed DJF (left) SST anomalies (°C), (center) precipitation anomalies (mm day^{-1}), and (right) 200-hPa height anomalies (contours; 8-m interval) for (top) EP El Niño, (middle) CP El Niño, and (bottom) their difference. Anomalies and differences that are statistically significant at the 95% confidence level with the *t* test are stippled. The outlined box shows the Niño-3 region bounded by 150°–90°W, 5°N–5°S.

statistically significant for any location within the contiguous United States, indicative of the strong sampling variability in El Niño surface climate composites (see also Deser et al. 2018).

b. *AMIP simulated signals for CP and EP El Niño events*

We turn our attention to the simulation ensembles seeking more robust evidence for distinct climate signals associated with the El Niño flavors than is possible from empirical analysis alone. The GFSv2 AMIP simulations confirm that observed large-scale differences in tropical Pacific precipitation anomalies between EP and CP composites are symptomatic of a sensitivity to their different SST forcings (cf. middle panels of Figs. 4 and 2). Specifically, greater positive SST anomalies in the far eastern Pacific during EP events induce an eastward displacement of maximum equatorial

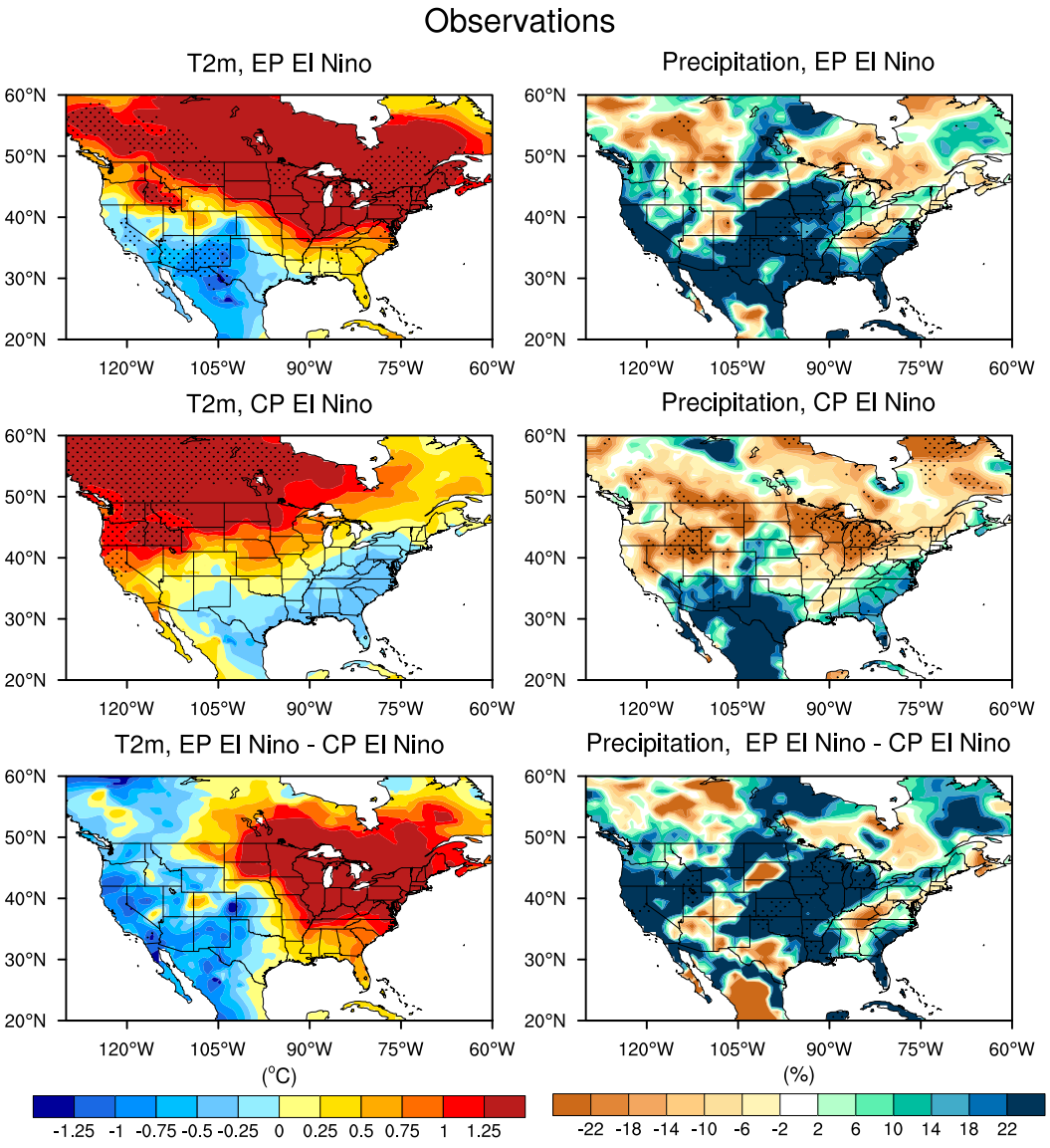

FIG. 3. Composite of observed DJF (left) surface air temperature anomalies (°C) and (right) precipitation anomalies (percent departures) for (top) EP El Niño, (middle) CP El Niño, and (bottom) their difference. Anomalies and differences that are statistically significant at the 95% confidence level with the *t* test are stippled.

positive precipitation anomalies. The GFSv2's close agreement with the observed tropical rainfall composites affirms the model's realism of this first link in the atmospheric teleconnection process.

To better understand how the pattern and magnitude of El Niño SST warming affects tropical Pacific rainfall, we present zonal cross sections of the simulated near-equatorial precipitation anomalies for each of the 11 El Niño events since 1979, ranked from the weakest (top) to the strongest (bottom) event based on a conventional Niño-3.4 metric (Fig. 1). It is immediately clear that only 2 of the 11 events, the very strong 1982/83 and 1997/98 events that are both EP cases, generate appreciably positive rainfall anomalies east of 120°W (the centroid of Niño-3 region). This indicates that only the very large amplitude El Niño warmings create an atmospheric response of large rainfall over the far eastern equatorial Pacific, highlighting the importance of El Niño amplitude and the nonlinearities inherent in the SST–rainfall relationship for that region. For the top seven ranked weaker El Niño events that include the 2014/15 CP and 2006/07 EP events of the weak Niño-3.4 amplitude and the 2009/10 CP event of moderate Niño-3.4 amplitude, there is practically no rainfall enhancement in the region

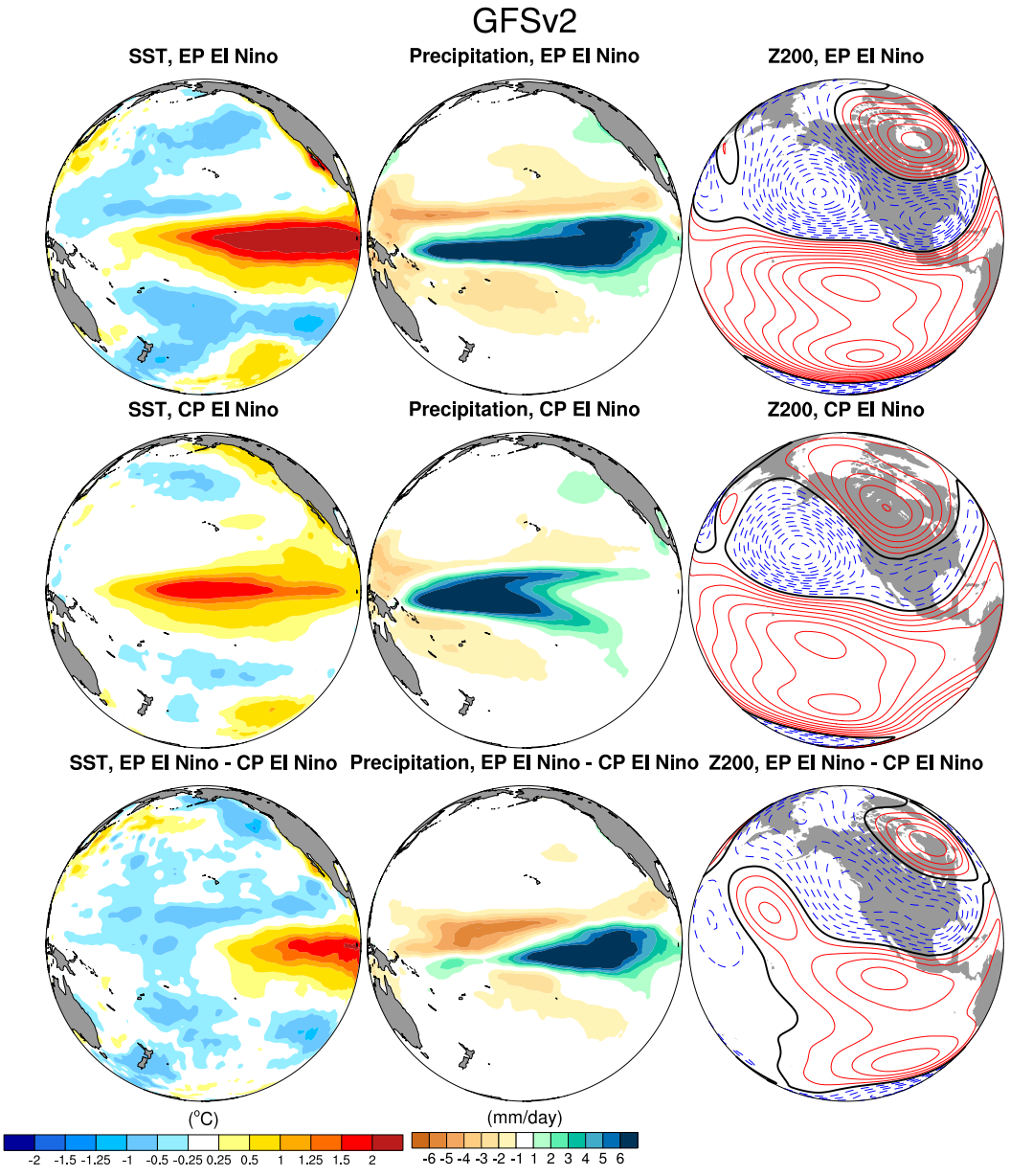

FIG. 4. Composite of (left) observed DJF SST anomalies (°C) and GFSv2 simulated 50-member ensemble mean DJF (center) precipitation anomalies (mm day^{-1}) and (right) 200-hPa height anomalies (contours; 8-m interval) for (top) EP El Niño, (middle) CP El Niño, and (bottom) their difference. Precipitation shaded values and circulation anomalies and differences with magnitude greater than about 10 m are statistically significant at the 95% confidence level with the *t* test.

east of 120°W. These seven El Niño events, regardless of whether they are distinguished by their patterns being either EP or CP type, have similar rainfall patterns along the equatorial eastern Pacific. Precipitation is only different among them in the central Pacific with a primary rainfall enhancement occurring west of the date line for the weaker events and slightly east of the date line for more moderate events.

There are also indications for the importance of spatial patterns of the SST anomalies. The two strong El Niño events (1982/83 and 1997/98) combine idiosyncratic features of both their amplitude and their spatial pattern, making it difficult to divorce these two elements. But noteworthy is the comparison of the equatorial profiles of SSTs and rainfall for the 1997/98 very strong EP event to the 2015/16 CP event, whose

magnitude of Niño-3.4 anomalies was actually greater. Yet, this CP event exhibits very little enhancement in rainfall over the far eastern equatorial Pacific, despite its Niño-3.4 magnitude ranking the second on record since at least 1980. The much weaker east equatorial Pacific rainfall enhancement in 2016 compared to 1998 is clearly inconsistent with a hypothesis that the atmospheric impacts are dictated by the amplitude of an event alone. Here it is evident that the pattern matters, and the contrast in the longitudinal profile of the SST anomalies in 2016 versus 1998 (see left panels of Fig. 1), which distinguishes CP from EP, is the unique feature of pattern distinction that is most relevant for these cases.

The results thus provide evidence that both El Niño amplitude and El Niño pattern matter for the atmospheric impacts. They also clarify that the large amplitude EP events dictate the eastern equatorial Pacific precipitation differences between EP and CP composites. The weak amplitude EP event behaves, with regard to tropical precipitation, more like the CP events than the very strong EP events. Further, CP events are more consistent in their tropical rainfall anomaly patterns among the individual cases, indicating that the CP composite is more homogeneous. Our argument aligns with Garfinkel et al. (2019), who noted the importance of SST anomaly magnitudes, demonstrating the appreciable contrast of the eastern equatorial Pacific (and U.S.) precipitation sensitivity to moderate versus strong EP forcing.

The dynamical effect of this zonal shift in equatorial Pacific rainfall is to displace the subtropical and extratropical wave train pattern eastward (Fig. 4, right). The simulated wintertime tropospheric signal of CP events resembles more the classic Pacific–North American (PNA) teleconnection while that associated with EP events resembles the tropical–Northern Hemisphere (TNH) teleconnection (see Mo and Livzey 1986). The magnitude of the composite circulation anomalies for the EP events is also greater, consistent with the larger equatorial Pacific warm SST anomalies and their associated tropical rainfall anomalies. Although the similarity of circulation differences of EP versus CP between the model and observations is strong, a close inspection reveals a slight difference in the position and magnitude of the cyclone circulation over the U.S. west coast (bottom right of Figs. 2 and 4), which is accompanied by some minor differences in the meridional wind anomalies, particularly along the coast of western Canada (not shown). It is likely that sampling variability plays a role in this distinction of circulation differences of EP versus CP between model and observations. A qualitative judgement on the model's realism can be drawn from two indirect indications. One is the expectation from linear theory for an eastward shifted extratropical wave train in response to an eastward shift in tropical Pacific convection (Hoskins and Karoly 1981; Ting and Sardeshmukh 1993). The other is the reproduction of the GFSv2 differences using a second ensemble suite of AMIP experiments based on a second model, CAM5. The composite circulation anomalies derived from those identical atmospheric model experiments again reveal a larger amplitude, eastward shifted extratropical wave train during EP relative to CP events (see Fig. A1 in the appendix).

Having identified the basis for, and having revealed the structure of, different atmospheric teleconnections associated with CP and EP events, we now examine the extent to which they induce different impacts on U.S. wintertime precipitation and temperature (Fig. 5). The distinctive features in common for both events are the meridional dipole patterns consisting of northern U.S. warmth/dryness and southern U.S. coolness/wetness. These common elements of U.S. impacts for both El Niño types are also broadly visible in the observational composites. The most prominent distinction between their composite signals is that EP events are colder and wetter across much of the contiguous United States. The wetter/colder U.S. climate during EP events is due to a spatial change in patterns, rather than due to a mere amplitude modulation of a single (CP) pattern. For instance, colder U.S. conditions during EP events arise from a northward displacement in the meridional dipole of the temperature anomaly pattern occurring in CP cases. This is generally true also for the wetter U.S. conditions during EP events, although a stronger wet signal in the American Southwest also results from a farther eastward extension of the Pacific storm track during EP El Niño.

These surface climate differences overall are physically explained by the fact that EP events (especially for the strong cases) exhibit a large-scale cyclonic circulation spanning most of the United States relative to the CP composite (Fig. 4, lower right), a feature that would favor coolness and wetness. In winter, since meridional advection plays an important role in temperature anomalies, a cyclonic circulation would be expected to result in cooler temperatures on its western flank and warmer temperatures on its eastern flank, as seen from Fig. 5 (lower left). For the precipitation anomalies, the circulation differences consisting of stronger westerlies across the U.S. West Coast (Fig. 4, bottom right) imply stronger zonal advection of moisture from the Pacific and enhanced storminess resulting in increased precipitation there. Enhanced westerlies span the entire southern U.S. region including the Gulf of Mexico, thus also favoring increased storminess and greater

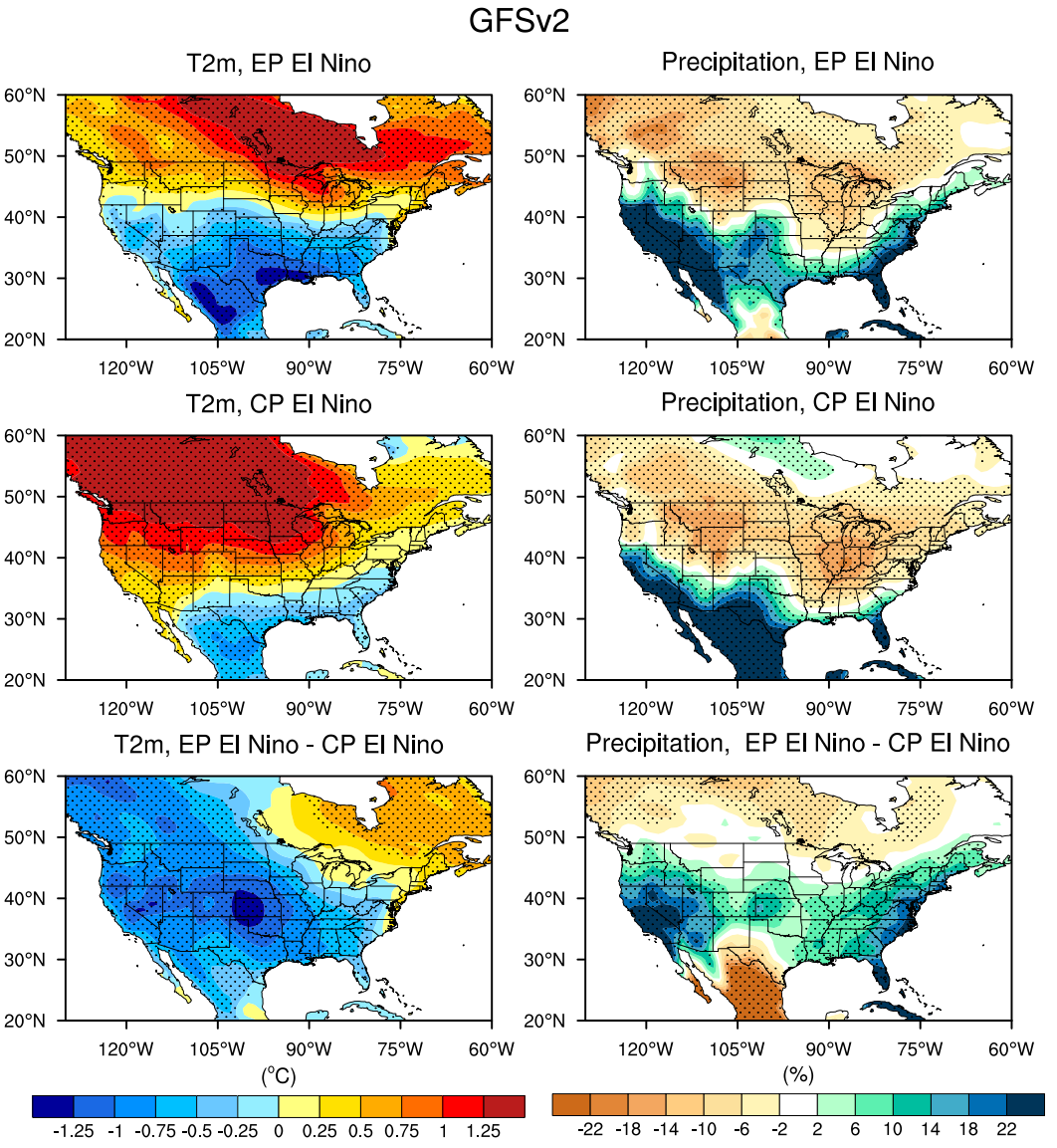

FIG. 5. As in Fig. 3, but for the GFSv2 simulated 50-member ensemble mean.

precipitation over the southeast United States. The colder surface temperature over the southern United States in the EP composite is likely also due to reduced incident solar radiation in this region associated with the increased precipitation (Zhang et al. 2011).

AMIP simulations based on a second model, CAM5, largely confirm the results based on the GFSv2 experiments. In particular, the CAM5 ensemble-mean results (Fig. A2) also reveal that the EP composite is colder and wetter over the contiguous United States, and likewise possesses several of the regional features identified in GFSv2.

We have also repeated the GFSv2 analysis but constructing the EP and CP composites based on the different event criteria of Table 1. For instance, a unanimity method that requires all three formulations to identify the same years as being either EP or CP leads to two EP classifications (1982/83 and 1997/98) and four events with CP classifications (1994/95, 2002/03, 2009/10, and 2014/15). The simulated U.S. temperature and precipitation composites for this sample (not shown) are very similar to those based on the majority consensus sampling used to construct Fig. 5. As further demonstrated in Fig A3, the result that the EP composite is colder/wetter over the contiguous United States, together with the key aforementioned regional features, is robust to using the three different methods of El Niño type classification. The principal sensitivity to the

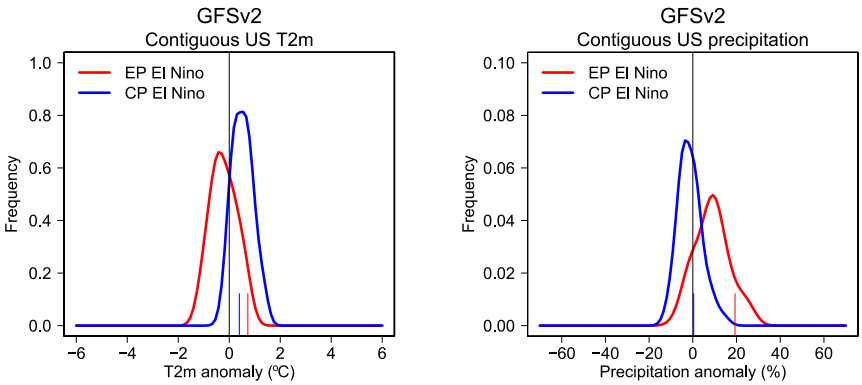

FIG. 6. PDFs of contiguous U.S. DJF (left) surface air temperature anomalies (°C) and (right) precipitation anomalies (percent departure) for EP El Niño (red curves) and CP El Niño (blue curves). El Niño case results are based on 50-member GFSv2 AMIP simulations subjected to global SST forcing. Large tick marks at the bottom show observed values for the composites of EP El Niño (red) and CP El Niño (blue). The PDFs are nonparametric curves utilizing kernel density estimation with a Gaussian smoother.

method of classification, and thus to the choice of samples included in each composite, concerns the magnitude of U.S. impacts.

Most of the U.S. pattern differences between the simulated EP and CP impacts are statistically significant, contrary to the observational composites for which few significant differences were found (cf. bottom panels of Figs. 3 and 5). This stems primarily from using large ensemble sizes in the model analysis that facilitate separation of signal from noise and is not necessarily due to a greater sensitivity to SST forcings in the model than in observations. To illustrate this, and to also offer a more informed assessment of the observational composites themselves, probability density functions (PDFs) of the 50 samples of GFSv2 simulated composite anomalies are constructed for contiguous U.S. averaged temperature and precipitation (Fig. 6). One principal feature is the appreciable spread of each PDF relative to its mean anomaly, indicating modest signal-to-noise ratios. The single observed composite samples are shown by long tick marks, which for temperature could plausibly have been drawn from either EP or CP histograms (left panel). In this sense, the observational composites, which indicate EP events to be warmer than CP events for the United States overall, are not representative (perhaps unluckily) of the true effect of El Niño diversity. By contrast, the observed precipitation composites do appear to align with the modeled signal diversity (perhaps fortuitously). The second principal feature of the histograms is their significant differences (based on a Kolmogorov–Smirnov test at 95% confidence) for EP composites (red curves) versus CP composites (blue curves). Despite the aforementioned sampling uncertainty, the availability of large ensembles used herein permits robust appraisal that the EP composite (associated especially with strong events) is colder and wetter than the CP composite for spatial averages over the contiguous United States.

c. *Predictability of impacts of CP and EP El Niño events from a coupled model*

The principal novelty of our work is that we use a coupled model based on an identical AGCM to establish the reliability for the AGCM-derived sensitivity shown in the previous section. The shortest lead coupled predictions retain virtually the same SST anomalies as we specify in the AGCM, which makes for meaningful intercomparison. As a matter of completeness, we examine the coupled model for their longer leads also in order to address predictability.

Shown in Fig. 7 are results based on a 24-member ensemble of CFSv2 1-month-lead hindcasts. Notable, and not surprising given the short lead time, is the model's ability to predict the principal feature distinguishing EP and CP SSTs, namely the greater far east Pacific warming of the former (cf. Figs. 2 and 7). Important is that the tropical Pacific rainfall differences associated with these predicted SST differences are very similar to those produced in the atmospheric models (cf. Figs. 4 and 7). Affirmed hereby is that the first leg in the teleconnection process distinguishing EP and CP composites can be understood as resulting from an atmospheric sensitivity to their diverse SST forcings. Likewise, the differences in upper-level heights between EP and CP events in the CFSv2 hindcasts are largely indistinguishable from those simulated in the AMIP experiments. We thus confirm the realism, in principle, of atmospheric responses to EP and CP composites

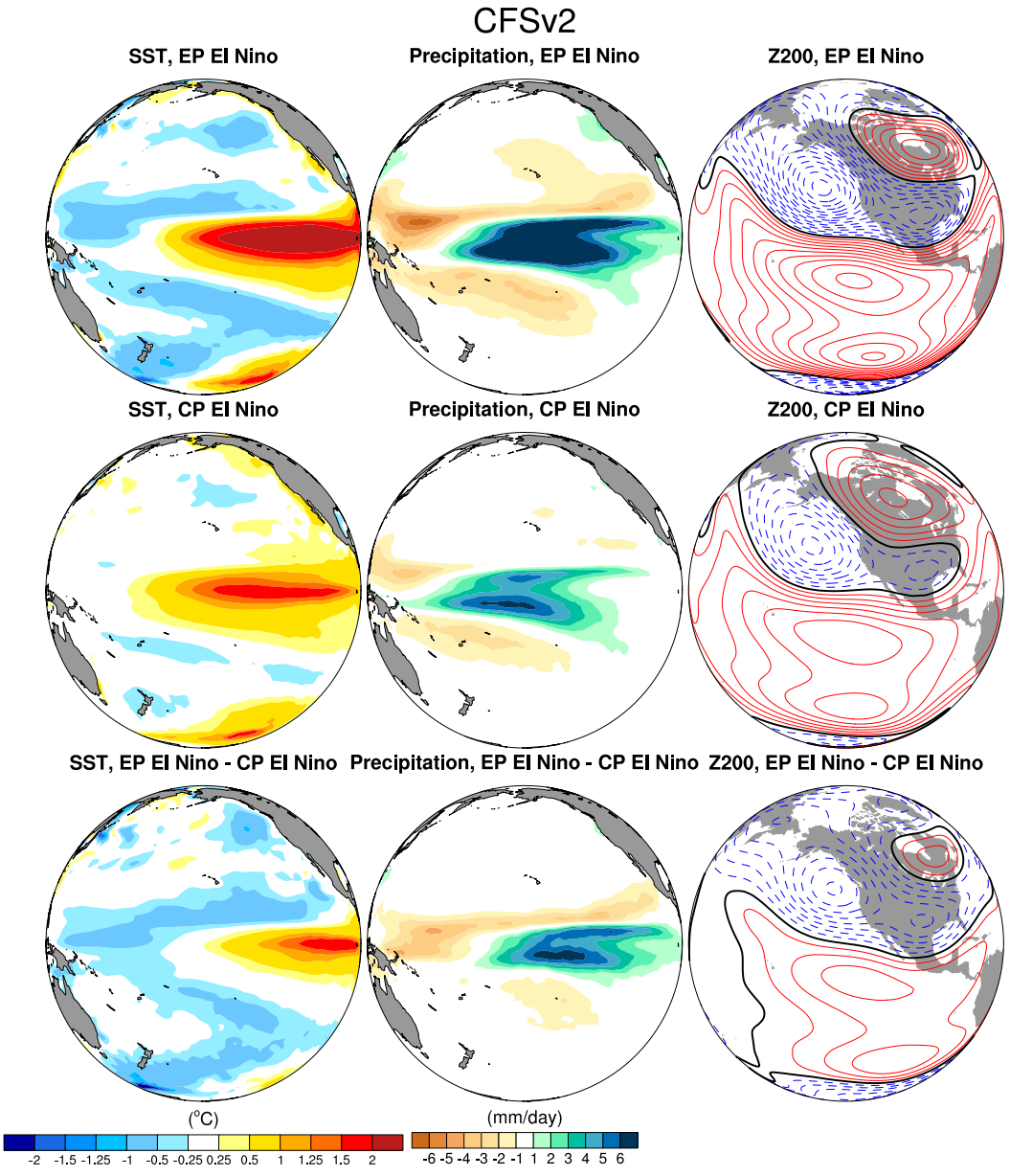

FIG. 7. Composite of DJF (left) SST anomalies (°C), (center) precipitation anomalies (mm day^{-1}), and (right) 200-hPa height anomalies (contours; 8-m interval) from a 24-member ensemble-mean 1-month-lead CFSv2 seasonal forecast based on October initializations for (top) EP El Niño, (middle) CP El Niño, and (bottom) their difference. The El Niño events used for the composite are the same as those for the observed composite. SST and precipitation shaded values and circulation anomalies and differences with magnitude greater than about 10 m are statistically significant at the 95% confidence level with the *t* test.

occurring in AGCM experiments. The parallel experiments employed herein give evidence that uncoupled modeling approaches, so extensively used in past studies, do not necessarily by reasons of their design distort the nature of air–sea interactions that drive differences in atmospheric impacts resulting from El Niño diversity.

Key for driving that teleconnection, and thus central to U.S. predictability, is a forecast model's ability to distinguish EP versus CP tropical Pacific SSTs and their effects on overlying east equatorial Pacific convection. Using Niño-3 area averaged SST and rainfall differences between EP and CP composites as indicator for skill in predicting these principal teleconnection forcings, we

summarize in Table 2 the lead-dependent performance of the CFSv2 hindcasts. The 0-lead predictions are virtually indistinguishable from the AMIP results, and are also close to observations. Statistically significant differences in the forecast EP versus CP SST composites are evident to 6-month lead. However, significant east equatorial Pacific rainfall differences are only predicted to 3-month lead. The combination of the weakening amplitude of the SST differences and the development of cold SST biases in the Niño-3 region (see supplemental Fig. S1) acts to inhibit the generation of convection and thus the rainfall sensitivity to El Niño flavors. For all practical purposes, distinct atmospheric teleconnections of the type observed that distinguish EP and CP events are no longer being driven in the forecast beyond 3 months.

The predictability of distinct U.S. impacts of El Niño flavors is assessed in Fig. 8 and Table 3. We find considerable agreement between AMIP and CFSv2 spatial distributions of U.S. surface temperature and rainfall composites at 1-month lead. This largely follows from the agreement previously noted among their tropical Pacific–extratropical teleconnections. For the United States overall, EP composites are colder and wetter in the CFSv2 hindcast as also found in the GFSv2 simulations, consistent with a general cyclonic circulation over the western United States in EP versus CP composites (see Fig. 7, bottom right).

The predictability of two key regional features that distinguish composite EP versus CP U.S. impacts is assessed in Table 3. One is the aforementioned contrast in west–east patterns of wintertime U.S. temperature with EP colder in the west and warmer in the east (see Figs. 3 and 5). The EP minus CP difference in surface temperature averaged over the western (west of 95°W) compared to the eastern United States (east of 95°W) is significantly negative at up to 2-month lead. The second feature is the appreciably wetter southwestern United States in EP relative to the CP composite. This feature is well reproduced in the forecast system to about 3-month lead. The outward loss of realism and skill in distinguishing EP versus CP regional impacts beyond 3 months is consistent with the loss in skill in predicting the tropical east Pacific rainfall differences. An apparent return of skill at 6-month lead can also be seen in Table 3, which we interpret as being coincidental and not representative of the teleconnection forcings that are actually responsible for EP versus CP composite differences.

As a final assessment of regional distinctions in effects of El Niño diversity, Figs. 9 and 10 compare the histograms of the GFSv2 AMIP simulations (left panels) to the 1-month-lead CFSv2 predictions (right panels). For anomalies in surface temperature (Fig. 9), the western United States is about 0.5°C colder than the eastern United States during EP versus CP (Fig. 9), a distinction seen in both the AMIP simulations (left) and the 1-month-lead predictions (right). For anomalies in precipitation (Fig. 10), the U.S. Southwest is appreciably wetter in the EP composite compared to the CP composite, again with excellent agreement between the atmospheric model simulations and the coupled model 1-month-lead predictions. Affirmed hereby is the suitability of the AMIP approach for discerning the different regional climates of EP versus CP El Niño events, and also the considerable predictability of the different El Niño types and their impacts, at least at short leads.

TABLE 2. The EP minus CP differences in SSTs (°C) and rainfall (mm day^{-1}) for observations, GFSv2 50-member AMIP simulations, and CFSv2 24-member hindcasts from 0- to 6-month leads. Differences are calculated for the Niño-3 region (150°–90°W, 5°N–5°S). Boldface numbers indicate differences that are significant at a 95% confidence level with the *t* test.

	Difference in SST anomalies between EP and CP events (°C)	Difference in precipitation anomalies between EP and CP events (mm day^{-1})
Obs	1.25	3.78
GFSv2	1.25	**4.56**
0-month lead	**1.24**	**4.13**
1-month lead	**1.12**	**3.27**
2-month lead	**1.01**	**2.03**
3-month lead	**0.79**	**0.85**
4-month lead	**0.36**	−0.15
5-month lead	**0.47**	−0.011
6-month lead	**0.60**	0.36

4. Summary and discussion

Motivated by observational indications that different flavors of El Niño may have exerted different impacts on wintertime U.S. temperature and precipitation, AMIP simulations during 1980–2018 have been diagnosed to explore the basis for event dependency. We used two atmospheric models, both with at least 40 members, to determine if distinct U.S. signals associated with two particular El Niño flavors, CP and EP events, existed. A second model framework based on initialized coupled climate forecasts was used to assess the robustness of climate sensitivities in the uncoupled model approaches and to examine associated predictability.

We found the effects of composite EP El Niño events in the atmospheric model experiments to induce colder and wetter wintertime conditions for the contiguous United States than composite CP El Niño events.

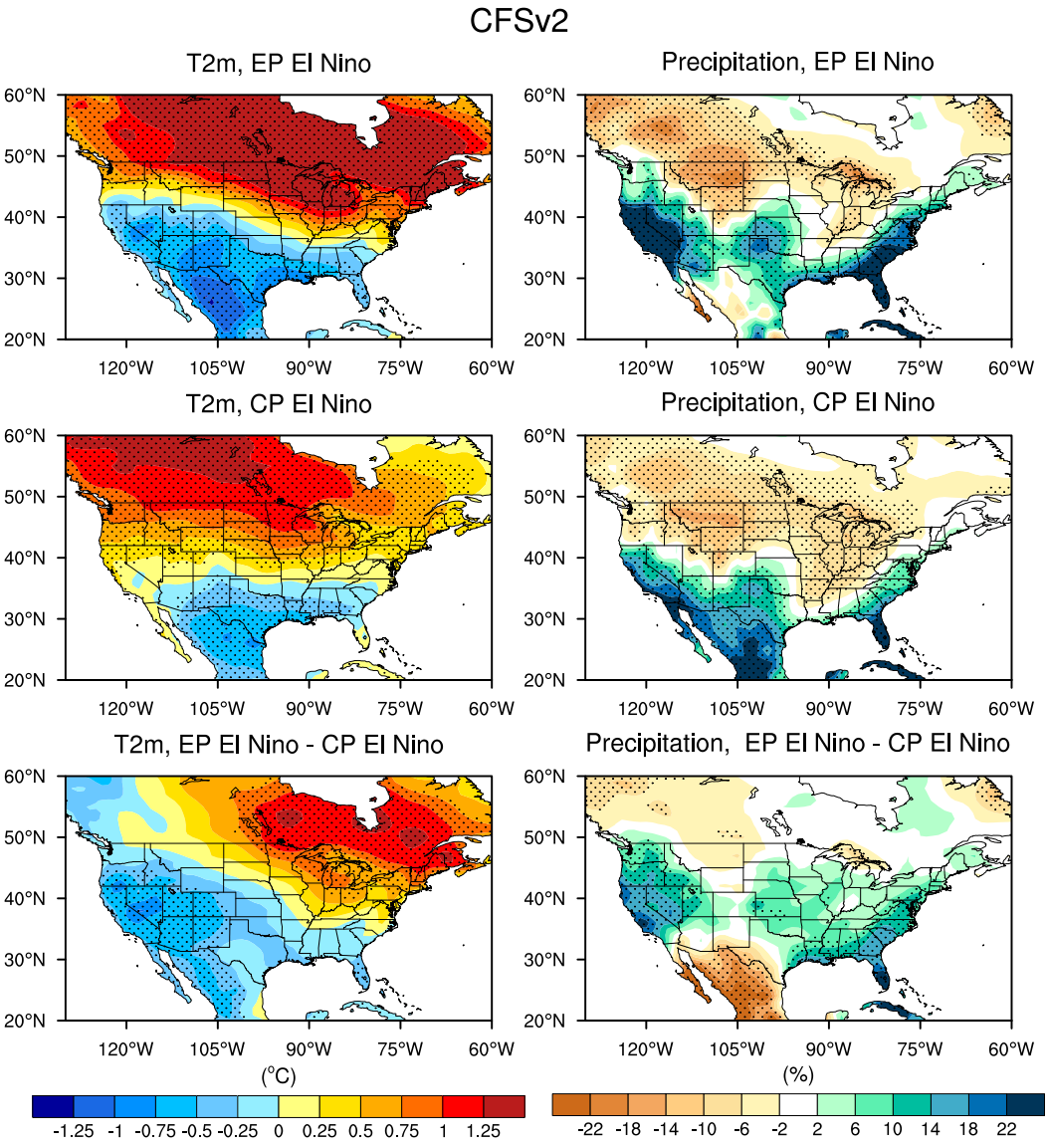

FIG. 8. As in Fig. 3, but for a 24-member ensemble-mean 1-month-lead CFSv2 seasonal forecast based on October initializations. The El Niño events used for the composite are the same as those for the observed composite.

Robust differences in their regional effects were identified that consisted of colder western and warmer eastern U.S. surface conditions and wetter southwestern and southeastern U.S. conditions associated with EP versus CP composites. These regional features were reproducible across two different atmospheric models studied herein, and also across various methods for characterizing EP and CP events. It is also noted that the EP event composite signals are most pronounced under stronger EP forcing during which an enhancement of eastern Pacific convection occurs—the EP composite may not be particularly applicable to describing the signals associated with weak EP events which appear more consistent with CP events. The patterns of U.S. temperature and precipitation differences between EP and CP composites based on our simulations specifying realistic observed SST anomalies in atmospheric models are qualitatively consistent with those found in similar modeling experiments of Hu et al. (2012) and Garfinkel et al. (2019). Important is that our parallel analysis of EP versus CP atmospheric impacts using a coupled ocean–atmosphere model confirmed the realism of the sensitivities that have heretofore relied solely on uncoupled modeling approaches.

TABLE 3. The EP minus CP differences in U.S. surface air temperature (°C) and precipitation (departures as percent of climatology) for observations, GFSv2 50-member AMIP simulations, and CFSv2 24-member hindcasts from 0- to 6-month leads. Temperature differences are calculated as the differences in anomalies averaged over the land areas of the western United States (west of 95°W) and those averaged over the land areas of the eastern United States (east of 95°W). Precipitation differences are calculated over the southwest land area bounded by 32°–39°N, 125°–112°W. Boldface numbers indicate differences that are significant at a 95% confidence level with the *t* test.

	Difference in U.S. surface air temperature zonal gradient between EP and CP events (°C)	Difference in Southwest precipitation anomalies between EP and CP events (%)
Obs	−1.47	39.80
GFSv2	**−0.50**	**23.34**
0-month lead	**−0.89**	**17.06**
1-month lead	**−0.56**	**13.28**
2-month lead	**−0.40**	7.30
3-month lead	**0.21**	**13.78**
4-month lead	−0.11	−2.64
5-month lead	**−0.12**	0.99
6-month lead	**−0.45**	**11.78**

A physical basis for distinct EP versus CP U.S. impacts was established by tracking the entire teleconnection chain linking differences in tropical SSTs to atmospheric circulation. First, the two El Niño flavors induce different tropical precipitation anomalies—enhanced equatorial Pacific convection during EP events is farther east than for CP events. Further analysis reveals that it is the large amplitude EP events that dictate the eastern equatorial Pacific precipitation differences between EP and CP event composites. The weak amplitude EP events behave more like the CP events, while CP events are more consistent in their tropical rainfall anomaly patterns among the individual cases and the CP composite is thus more homogeneous. In response to the different tropical precipitation anomalies of the two El Niño flavors, upper-tropospheric atmospheric circulation anomalies—in particular, the longitudes of anomalies in the subtropical Pacific highs, North Pacific lows, and North American highs—are eastward displaced during EP relative to CP events. These differences in wave trains are consistent with predictions from linear dynamical models given the shift in tropical convection (Ting and Sardeshmukh 1993). Likewise, the differences in U.S. precipitation and temperature patterns are consistent with expected storm track sensitivities to these different circulation patterns (Hoerling and Ting 1994). The generally colder and wetter U.S. conditions during EP events are shown to be a consequence of the fact that the EP composite exhibits a large-scale cyclonic circulation spanning most of the United States relative to the CP composite.

We explored the predictability of El Niño flavors and related U.S. climate impacts in an initialized coupled forecast system. We found high SST prediction skill in distinguishing El Niño flavors at short

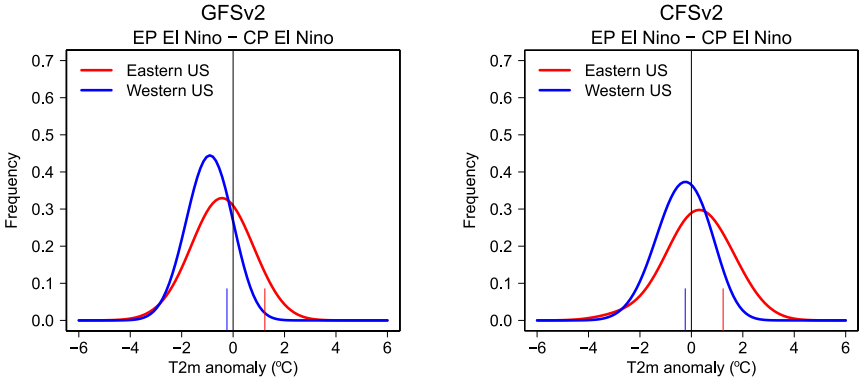

FIG. 9. PDFs of regional U.S. DJF surface air temperature differences (EP – CP) for the western (blue curve) and eastern (red curve) United States. Results are compared for (left) the 50-member GFSv2 AMIP simulations and (right) the 24-member CFSv2 1-month-lead hindcasts. Note that the curves for GFSv2 and CFSv2 are constructed by a sample size of 2500 and 576, respectively, of composites based on the respective resampling of 50 and 24 EP and CP composites. Large tick marks at the bottom show observed values. The PDFs are nonparametric curves utilizing kernel density estimation with a Gaussian smoother. The western and eastern United States are defined to be the land areas west of and east of 95°W, respectively.

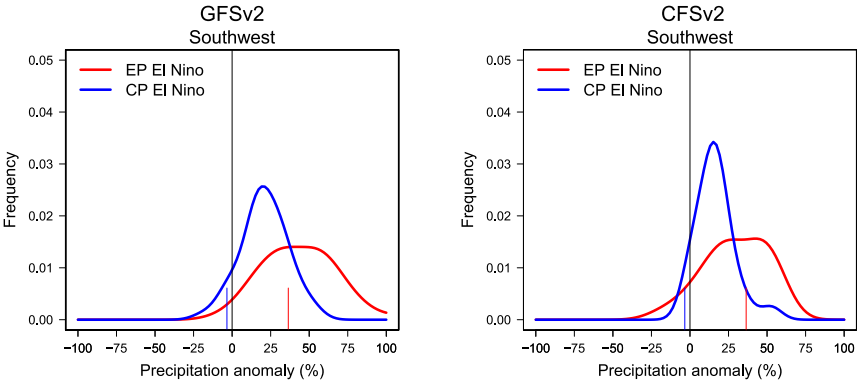

FIG. 10. PDFs of regional DJF precipitation anomalies (percent departure) over the southwest land area bounded by 32°–39°N, 125°–112°W for EP El Niño (red curve) and CP El Niño (blue curve). Results are compared for (left) the 50-member GFSv2 AMIP simulations and (right) the 24-member CFSv2 1-month-lead hindcasts. Large tick marks at the bottom show observed values for the composites of EP El Niño (red) and CP El Niño (blue). The PDFs are nonparametric curves utilizing kernel density estimation with a Gaussian smoother.

leads (to about 3-month lead) using CFSv2 hindcasts. Skill vanishes after about 3 months, consistent with other studies that have shown the difficulty in forecasting different El Niño types with a lead time longer than a few months in operational prediction systems (Hendon et al. 2009; Kirtman et al. 2014). The CFSv2 skill is comparable to that reported in a recent study on winter predictability of ENSO types for six operational dynamical model systems (Ren et al. 2019), and we thus judge the CFSv2 results presented herein to be broadly representative of state-of-the-art forecast systems. The CFSv2 hindcasts also reproduced the regional U.S. patterns of distinct temperature and precipitation signals accompanying predicted EP and CP El Niño composites, thus further affirming the climate sensitivity of the AMIP simulations. At leads longer than about 3 months, a combination of reduced amplitudes in the predicted SST contrast of EP versus CP composites and growing cold SST biases in the equatorial east Pacific inhibits the generation of realistic teleconnections to North America.

Our results of significant differences in U.S. impacts associated with two patterns of SST warmings that reside under the broad category of El Niño events clarify several conjectures on ENSO teleconnections postulated by Horel and Wallace (1981). First, the pattern of the overall linear correlation between upper air geopotential heights with tropical Pacific SSTs does indeed constitute a blurred image of sharper patterns. Second, there is reason to expect that forecast systems that can distinguish the specific SST pattern (i.e., magnitude and spatial structure) of warm episodes would render more accurate prediction of midlatitude impacts, specifically regional structures of U.S. temperature and precipitation. We should nonetheless be cognizant that the modest linear correlations between ENSO and extratropical teleconnections are mostly due to internal variability in the extratropics, and can only be modestly reconciled with diversity in tropically forced atmospheric teleconnections (e.g., Hoerling and Kumar 2002).

In their recent study of U.S. seasonal predictability based on a 60-yr reforecast dataset, Huang et al. (2019) noted that ENSO was the principal source of U.S. seasonal skill in their forecast system. Harkening to the thoughts of Horel and Wallace (1981), they also noted the potential importance of diversity in responses to El Niño flavors for advancing seasonal forecast skill. In this sense, we view our current results as being a substantive step in a direction toward building confidence among seasonal forecast practitioners to incorporate U.S. impact patterns of El Niño events that discriminate according to EP and CP El Niño types. Although recognizing that individual events may not completely fall into either specific EP or CP category, and that careful scrutiny must be given to *both the magnitude and spatial pattern of SST anomalies*, it is our view that due consideration of this knowledge may help to fine-tune seasonal temperature and precipitation outlooks.

Acknowledgments. We thank Dr. Xiaowei Quan for carrying out the large CAM5 ensemble runs and Drs. Antonietta Capotondi and Joseph Barsugli and two anonymous reviewers for their constructive comments. This research was supported by federally appropriated funds.

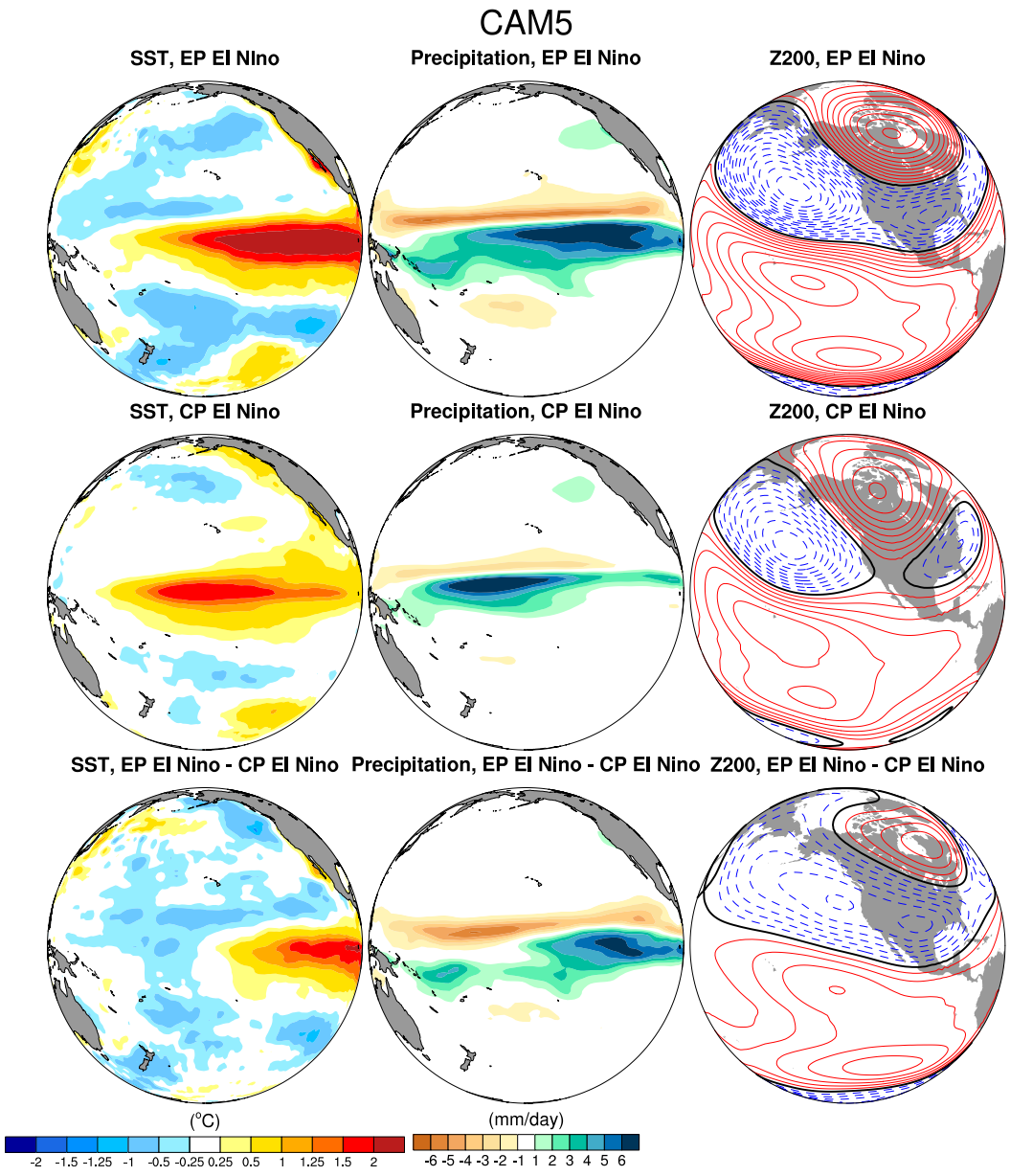

FIG. A1. Composite of (left) observed DJF SST anomalies (°C) and CAM5 simulated 40-member ensemble mean DJF (center) precipitation anomalies (mm day^{-1}) and (right) 200-hPa height anomalies (contours; 8-m interval) for (top) EP El Niño, (middle) CP El Niño, and (bottom) their difference. Precipitation shaded values and circulation anomalies and differences with magnitude greater than about 10 m are statistically significant at the 95% confidence level with the *t* test.

APPENDIX

Robustness of the Distinct U.S. Impacts of El Niño Flavors

To test the robustness of the distinct signals of EP versus CP events identified in GFSv2 AMIP simulations, we repeat the analysis by using the AMIP simulations from a different atmospheric model. Figure A1 shows that CAM5 ensemble-mean results can reproduce the key features revealed in GFSv2 that there is an eastward shift of maximum equatorial positive precipitation anomalies accompanied by a large amplitude and eastward displaced extratropical wave train during EP versus CP events as shown in Fig. 4. The CAM5 ensemble-mean results also confirm the robustness of

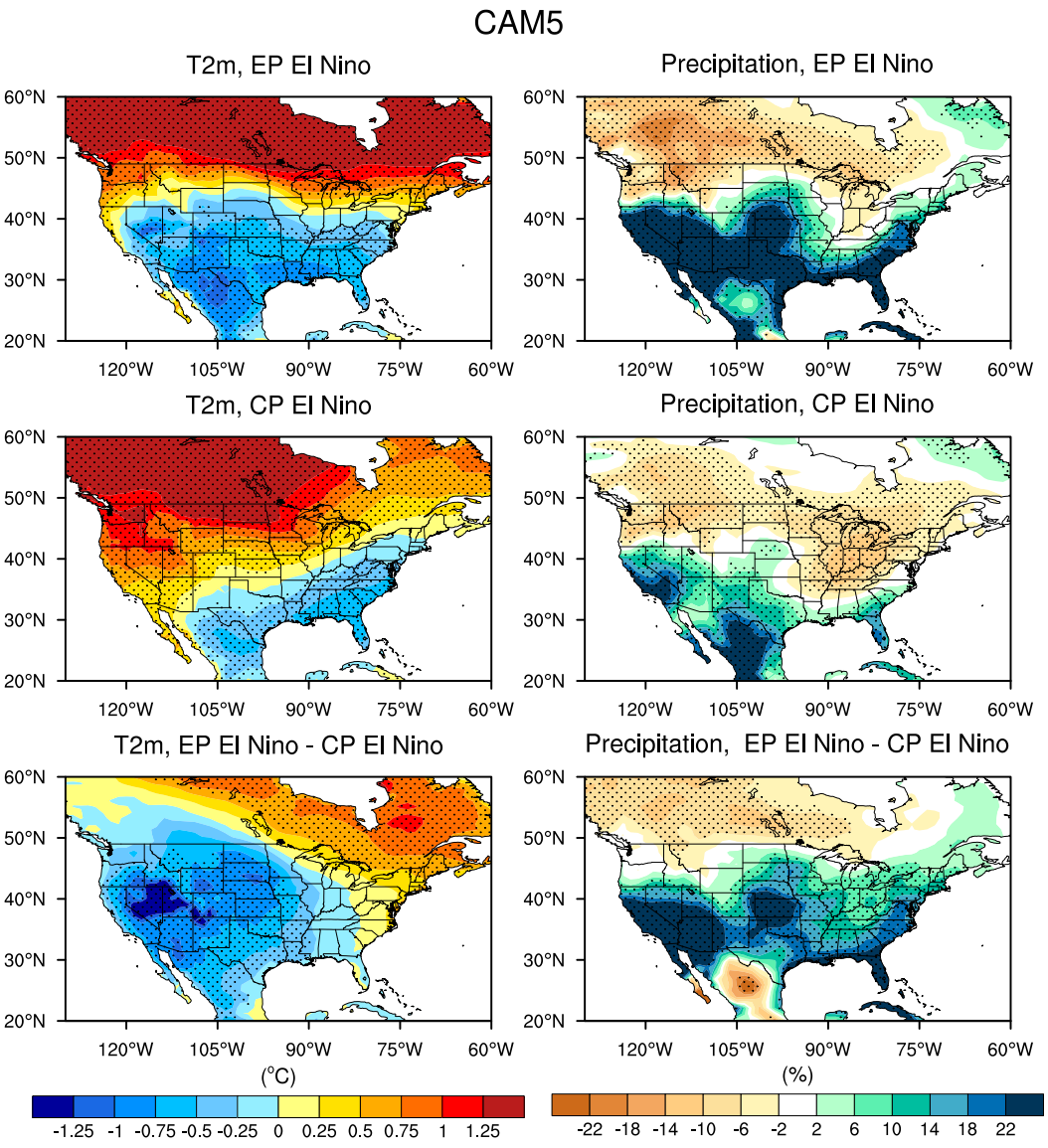

FIG. A2. As in Fig. 3, but for the CAM5 simulated 40-member ensemble mean.

different impacts of U.S. wintertime climate. A comparison between Fig. A2 and Fig. 5 shows that the agreement is strong, both in the spatial structures of two types of El Niño and in their differences. Specifically, the north–south contrast pattern of surface air temperature is dominant for both types of El Niño and a broad cooling is dominant over most U.S. regions for their differences. There are above-normal rains over the western and southern coast and below-normal rains elsewhere for both types of El Niño with a relatively broader wetting pattern for EP events compared to CP events. The results suggest that the signal of relative U.S. coldness and wetness during EP El Niño (in comparison with CP El Niño) is robust and does not depend on the selection of a particular atmospheric model.

As discussed in the method section, we focus on employing the majority method introduced by Yu et al. (2012) to define the two types of El Niño events in this study (Table 1). We assess whether the distinct U.S. impacts of El Niño flavors are sensitive to the method used to define the El Niño type. Figure A3 shows the differences in the GFSv2 ensemble-mean winter anomalies of surface air temperature (left panel) and precipitation (right panel) between EP and CP El Niño based on the Niño method of Yeh et al. (2009) (top row), the EMI method of Ashok et al. (2007) (middle row),

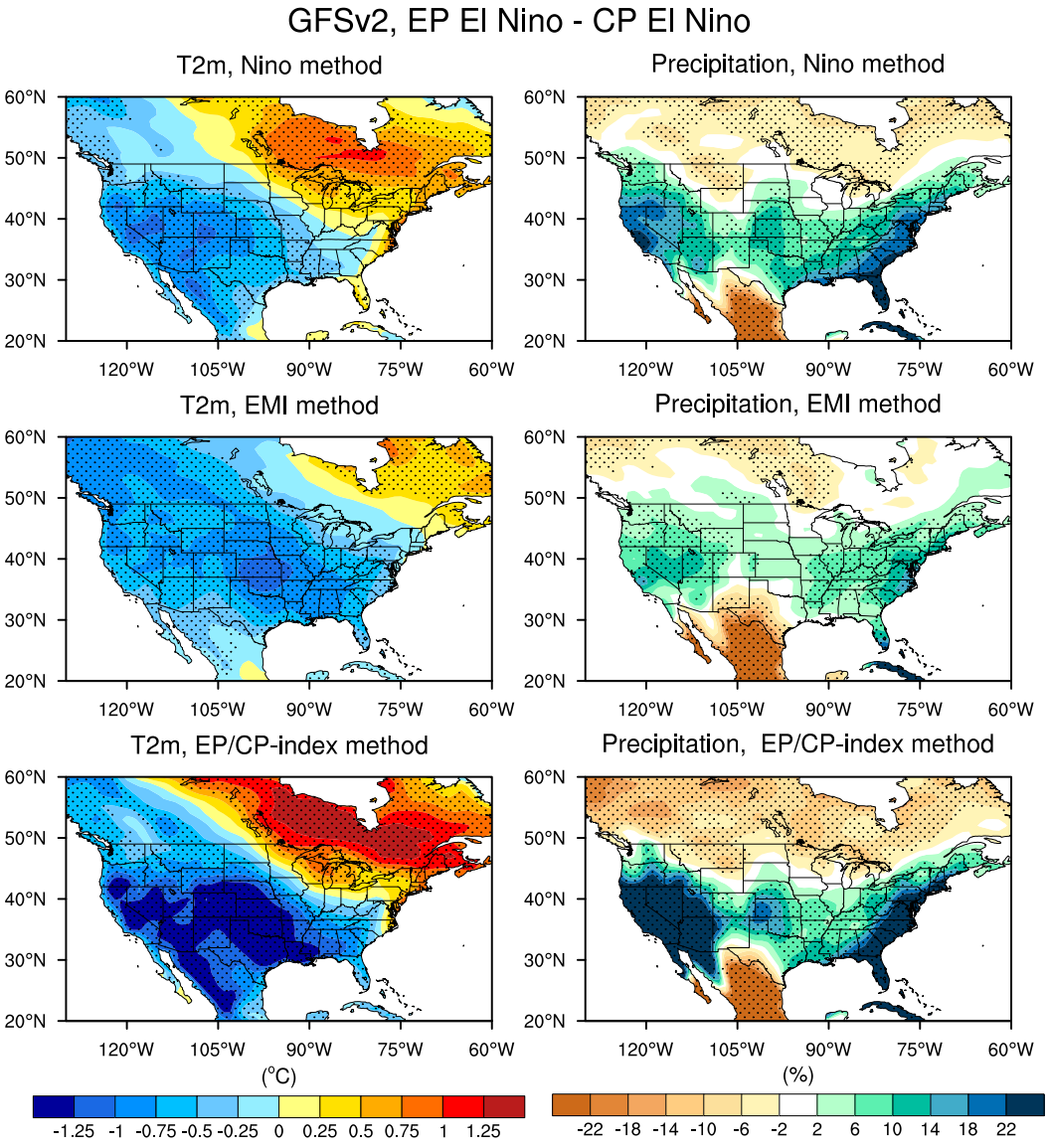

FIG. A3. The difference in the composite of GFSv2 simulated 50-member ensemble mean DJF (left) surface air temperature anomalies (°C) and (right) precipitation anomalies (percent departures) between EP and CP El Niño for the definition of El Niño type based on the (top) Niño method, (middle) EMI method, and (bottom) EP/CP-index method as listed in Table 1. Differences that are statistically significant at the 95% confidence level with the *t* test are stippled.

and the EP/CP index method of Kao and Yu (2009) (bottom row). It is clear that the three different methods yield very similar spatial patterns of surface climate anomalies for the differences between two types of El Niño, although the magnitude of the difference is strongest using the EP/CP index method and generally smallest using the EMI method. We have compared the results of Fig. A3 with those of Fig. 5 bottom and found that they are also very similar to each other, implying that the conclusion of a colder and wetter U.S. condition during EP El Niño than CP El Niño is robust and does not depend on the methods used to define the type of El Niño.

REFERENCES

Ashok, K., S. K. Behera, S. A. Rao, H. Weng, and T. Yamagata, 2007: El Niño Modoki and its possible teleconnection. *J. Geophys. Res.*, **112**, C11007, https://doi.org/10.1029/2006JC003798.

Barsugli, J. J., and P. D. Sardeshmukh, 2002: Global atmospheric sensitivity to tropical SST anomalies throughout the Indo–Pacific basin. *J. Climate*, **15**, 3427–3442, https://doi.org/10.1175/1520-0442(2002)015<3427:GASTTS>2.0.CO;2.

Capotondi, A., and Coauthors, 2015: Understanding ENSO diversity. *Bull. Amer. Meteor. Soc.*, **96**, 921–938, https://doi.org/10.1175/BAMS-D-13-00117.1.

Deser, C., I. R. Simpson, A. S. Phillips, and K. A. McKinnon, 2018: How well do we know ENSO's climate impacts over North America, and how do we evaluate models accordingly? *J. Climate*, **31**, 4991–5014, https://doi.org/10.1175/JCLI-D-17-0783.1.

Fan, Y., and H. van den Dool, 2008: A global monthly land surface air temperature analysis for 1948–present. *J. Geophys. Res.*, **113**, D01103, https://doi.org/10.1029/2007JD008470.

Garfinkel, C. I., M. M. Hurwitz, D. W. Waugh, and A. H. Butler, 2013: Are the teleconnections of central Pacific and eastern Pacific El Niño distinct in boreal wintertime? *Climate Dyn.*, **41**, 1835–1852, https://doi.org/10.1007/s00382-012-1570-2.

——, I. Weinberger, I. P. White, L. D. Oman, V. Aquila, and Y. K. Lim, 2019: The salience of nonlinearities in the boreal winter response to ENSO: North Pacific and North America. *Climate Dyn.*, **52**, 4429–4446, https://doi.org/10.1007/s00382-018-4386-x.

Guo, Y., M. Ting, Z. Wen, and D. E. Lee, 2017: Distinct patterns of tropical Pacific SST anomaly and their impacts on North American climate. *J. Climate*, **30**, 5221–5241, https://doi.org/10.1175/JCLI-D-16-0488.1.

Hartmann, D. L., 2015: Pacific sea surface temperature and the winter of 2014. *Geophys. Res. Lett.*, **42**, 1894–1902, https://doi.org/10.1002/2015GL063083.

Hendon, H. H., E. Lim, G. Wang, O. Alves, and D. Hudson, 2009: Prospects for predicting two flavors of El Niño. *Geophys. Res. Lett.*, **36**, L19713, https://doi.org/10.1029/2009GL040100.

Hoell, A., M. Hoerling, J. Eischeid, K. Wolter, R. Dole, J. Perlwitz, T. Xu, and L. Cheng, 2016: Does El Niño intensity matter for California precipitation? *Geophys. Res. Lett.*, **43**, 819–825, https://doi.org/10.1002/2015GL067102.

——, C. Funk, J. Zinke, and L. Harrison, 2017: Modulation of the southern Africa precipitation response to the El Niño Southern Oscillation by the subtropical Indian Ocean dipole. *Climate Dyn.*, **48**, 2529–2540, https://doi.org/10.1007/s00382-016-3220-6.

——, M. Barlow, T. Xu, and T. Zhang, 2018: Cold season southwest Asia precipitation sensitivity to El Niño–Southern Oscillation events. *J. Climate*, **31**, 4463–4482, https://doi.org/10.1175/JCLI-D-17-0456.1.

Hoerling, M. P., and M. Ting, 1994: Organization of extratropical transients during El Niño. *J. Climate*, **7**, 745–766, https://doi.org/10.1175/1520-0442(1994)007<0745:OOETDE>2.0.CO;2.

——, and A. Kumar, 2002: Atmospheric response patterns associated with tropical forcing. *J. Climate*, **15**, 2184–2203, https://doi.org/10.1175/1520-0442(2002)015<2184:ARPAWT>2.0.CO;2.

——, ——, and M. Zhong, 1997: El Niño, La Niña, and the nonlinearity of their teleconnections. *J. Climate*, **10**, 1769–1786, https://doi.org/10.1175/1520-0442(1997)010<1769:ENOLNA>2.0.CO;2.

——, and Coauthors, 2013: Anatomy of an extreme event. *J. Climate*, **26**, 2811–2832, https://doi.org/10.1175/JCLI-D-12-00270.1.

Horel, J. D., and J. M. Wallace, 1981: Planetary-scale atmospheric phenomena associated with the Southern Oscillation. *Mon. Wea. Rev.*, **109**, 813–829, https://doi.org/10.1175/1520-0493(1981)109<0813:PSAPAW>2.0.CO;2.

Hoskins, B. J., and D. J. Karoly, 1981: The steady linear response of a spherical atmosphere to thermal and orographic forcing. *J. Atmos. Sci.*, **38**, 1179–1196, https://doi.org/10.1175/1520-0469(1981)038<1179:TSLROA>2.0.CO;2.

Hu, Z.-Z., A. Kumar, B. Jha, W. Wang, B. Huang, and B. Huang, 2012: An analysis of warm pool and cold tongue El Niños: Air–sea coupling processes, global influences, and recent trends. *Climate Dyn.*, **38**, 2017–2035, https://doi.org/10.1007/s00382-011-1224-9.

Huang, B., C.-S. Shin, and A. Kumar, 2019: Predictive skill and predictable patterns of the U.S. seasonal precipitation in CFSv2 reforecasts of 60 years (1958–2017). *J. Climate*, **32**, 8603–8637, https://doi.org/10.1175/JCLI-D-19-0230.1.

Hurrell, J., J. Hack, D. Shea, J. Caron, and J. Rosinski, 2008: A new sea surface temperature and sea ice boundary dataset for the Community Atmosphere Model. *J. Climate*, **21**, 5145–5153, https://doi.org/10.1175/2008JCLI2292.1.

Kalnay, E., and Coauthors, 1996: The NCEP/NCAR 40-Year Reanalysis Project. *Bull. Amer. Meteor. Soc.*, **77**, 437–471, https://doi.org/10.1175/1520-0477(1996)077<0437:TNYRP>2.0.CO;2.

Kao, H.-Y., and J.-Y. Yu, 2009: Contrasting eastern-Pacific and central-Pacific types of ENSO. *J. Climate*, **22**, 615–632, https://doi.org/10.1175/2008JCLI2309.1.

Kiladis, G. N., and H. Diaz, 1989: Global climatic anomalies associated with extremes in the Southern Oscillation. *J. Climate*, **2**, 1069–1090, https://doi.org/10.1175/1520-0442(1989)002<1069:GCAAWE>2.0.CO;2.

Kirtman, B. P., and Coauthors, 2014: The North American Multimodel Ensemble: Phase-1 seasonal-to-interannual prediction; phase-2 toward developing intraseasonal prediction. *Bull. Amer. Meteor. Soc.*, **95**, 585–601, https://doi.org/10.1175/BAMS-D-12-00050.1.

Kug, J.-S., F.-F. Jin, and S.-I. An, 2009: Two types of El Niño events: Cold tongue El Niño and warm pool El Niño. *J. Climate*, **22**, 1499–1515, https://doi.org/10.1175/2008JCLI2624.1.

Larkin, N. K., and D. E. Harrison, 2005: On the definition of El Niño and associated seasonal average U.S. weather anomalies. *Geophys. Res. Lett.*, **32**, L13705, https://doi.org/10.1029/2005GL022738.

Mo, K. C., 2010: Interdecadal modulation of the impact of ENSO on precipitation and temperature over the United States. *J. Climate*, **23**, 3639–3656, https://doi.org/10.1175/2010JCLI3553.1.

——, and R. E. Livzey, 1986: Tropical–extratropical geopotential height teleconnections during the Northern Hemisphere winter. *Mon. Wea. Rev.*, **114**, 2488–2515, https://doi.org/10.1175/1520-0493(1986)114<2488:TEGHTD>2.0.CO;2.

Neale, R. B., and Coauthors, 2012: Description of the NCAR Community Atmosphere Model (CAM 5.0). NCAR Tech. Note NCAR/TN-486+STR, 274 pp., www.cesm.ucar.edu/models/cesm1.0/cam/docs/description/cam5_desc.pdf.

Quan, X., M. Hoerling, J. Whitaker, G. Bates, and T. Xu, 2006: Diagnosing sources of U.S. seasonal forecast skill. *J. Climate*, **19**, 3279–3293, https://doi.org/10.1175/JCLI3789.1.

Rasmusson, E. M., and T. H. Carpenter, 1982: Variations in tropical sea surface temperature and surface wind fields associated with the Southern Oscillation/El Niño. *Mon. Wea. Rev.*, **110**, 354–384, https://doi.org/10.1175/1520-0493(1982)110<0354:VITSST>2.0.CO;2.

Ren, H.-L., and Coauthors, 2019: Seasonal predictability of winter ENSO types in operational dynamical model predictions. *Climate Dyn.*, **52**, 3869–3890, https://doi.org/10.1007/s00382-018-4366-1.

Ropelewski, C. F., and M. S. Halpert, 1986: North American precipitation and temperature patterns associated with the

El Niño/Southern Oscillation (ENSO). *Mon. Wea. Rev.*, **114**, 2352–2362, https://doi.org/10.1175/1520-0493(1986)114<2352:NAPATP>2.0.CO;2.

Saha, S., and Coauthors, 2014: The NCEP Climate Forecast System version 2. *J. Climate*, **27**, 2185–2208, https://doi.org/10.1175/JCLI-D-12-00823.1.

Schneider, U., A. Becker, P. Finger, A. Meyer-Christoffer, M. Ziese, and B. Rudolf, 2014: GPCC's new land surface precipitation climatology based on quality-controlled in situ data and its role in quantifying the global water cycle. *Theor. Appl. Climatol.*, **115**, 15–40, https://doi.org/10.1007/s00704-013-0860-x.

Stern, W., and K. Miyakoda, 1995: Feasibility of seasonal forecasts inferred from multiple GCM simulations. *J. Climate*, **8**, 1071–1085, https://doi.org/10.1175/1520-0442(1995)008<1071:FOSFIF>2.0.CO;2.

Ting, M., and P. D. Sardeshmukh, 1993: Factors determining the extratropical response to equatorial diabatic heating anomalies. *J. Atmos. Sci.*, **50**, 907–918, https://doi.org/10.1175/1520-0469(1993)050<0907:FDTERT>2.0.CO;2.

Xie, P., and P. A. Arkin, 1997: Global precipitation: A 17-year monthly analysis based on gauge observations, satellite estimates, and numerical model outputs. *Bull. Amer. Meteor. Soc.*, **78**, 2539–2558, https://doi.org/10.1175/1520-0477(1997)078<2539:GPAYMA>2.0.CO;2.

Yeh, S.-W., J.-S. Kug, B. Dewitte, M.-H. Kwon, B. P. Kirtman, and F.-F. Jin, 2009: El Niño in a changing climate. *Nature*, **461**, 511–514, https://doi.org/10.1038/nature08316.

Yu, J.-Y., and Y. Zou, 2013: The enhanced drying effect of central-Pacific El Niño on US winter. *Environ. Res. Lett.*, **8**, 014019, https://doi.org/10.1088/1748-9326/8/1/014019.

——, ——, S. T. Kim, and T. Lee, 2012: The changing impact of El Niño on US winter temperatures. *Geophys. Res. Lett.*, **39**, L15702, https://doi.org/10.1029/2012GL052483.

Zhang, T., M. P. Hoerling, J. Perlwitz, D.-Z. Sun, and D. Murray, 2011: Physics of U.S. surface temperature response to ENSO. *J. Climate*, **24**, 4874–4887, https://doi.org/10.1175/2011JCLI3944.1.

——, ——, ——, and T. Xu, 2016: Forced atmospheric teleconnections during 1979–2014. *J. Climate*, **29**, 2333–2357, https://doi.org/10.1175/JCLI-D-15-0226.1.

——, and Coauthors, 2018: Predictability and prediction of the Southern California rains during strong El Niño events: A focus on the failed 2016 winter rains. *J. Climate*, **31**, 555–574, https://doi.org/10.1175/JCLI-D-17-0396.1.